European Polymer Journal 91 (2017) 315–325

Contents lists available at ScienceDirect

European Polymer Journal

journal homepage: www.elsevier.com/locate/europolj

# Electrohydrodynamic patterning in a curable resin over a wide range of fabrication parameters

Claire H. Trease, Peter J.S. Foot*, Andy T. Augousti

*Faculty of Science, Engineering and Computing, Kingston University, London KT1 2EE, UK*

ARTICLE INFO

*Keywords:*
EHD instability patterning
Microlithography
Epoxy resin
Surface modification
Antireflection coating

ABSTRACT

This work reports the first use of a room-temperature curing epoxy resin to produce microscopic arrays of ordered 2-D structures via electrohydrodynamic instability (EHD) patterning. The measured spacing of these structures, and the formation of novel 'starburst' shapes, support a leaky dielectric theoretical model over perfect dielectric ones. The existence of the starbursts implies that traces of ionic residues in the uncured epoxy should be taken into account in any model of the patterning process, and their formation implies that mobile surface charges arising from trace ionic impurities must be considered when seeking to achieve smaller length-scale structures in epoxy by EHD using flat electrodes. Samples patterned in the μm range showed mid-infrared spectral features with wavelength maxima that broadly scaled with the pillar spacings in the films.

## 1. Introduction

Patterning polymers at the micro- and sub-micrometre scale has applications in a large and diverse range of fields from diffraction gratings and optical lenses, to tissue culture, sensing devices and even the treatment of surfaces to prevent the build-up of ice crystals [1–3].

Surface structures at these scales are generally produced by techniques such as photolithography and nano-imprint lithography. Typically, a photo-mask pattern is transferred to a photoresist material in order to protect areas of a silicon wafer prior to etching and the production of devices or moulds. These kinds of technologies are capable of achieving high resolution and reproducibility, but can sometimes be expensive and equipment-heavy, and many studies are being conducted into ways of fabricating micro- and nano-structured surfaces by simpler and cheaper technologies.

The technique of using an electric field to destabilise the interface between two fluid layers has been broadly understood for many decades, but in recent years there have been developments in its use as a micro- and nanoscale fabrication method called electrohydrodynamic (EHD) instability patterning. Most of this work has been done with thermoplastic polymers, especially poly (methyl methacrylate) (PMMA) and polystyrene (PS), but other materials have also been used, such as UV-curing polymers and sol-gels [4–7].

In EHD patterning, a fluid is applied to one electrode in a flat plate capacitor which is separated from the second electrode by an insulator such as air (Fig. 1A). A voltage is applied across the two electrodes, which creates an electric field both in the polymer and the insulator. It is the mismatch between these two fields that creates an electrostatic pressure at the interface and destabilises the surface of the fluid (Fig. 1B). Pillars or disks can then form, and when the fluid is solidified the structures are permanent (Fig. 1C).

A range of wavelengths initially exists at the interface, which grow in amplitude at different rates. The interaction between

* Corresponding author.
*E-mail address:* p.j.foot@kingston.ac.uk (P.J.S. Foot).

http://dx.doi.org/10.1016/j.eurpolymj.2017.04.011
Received 23 December 2016; Received in revised form 23 March 2017; Accepted 11 April 2017
Available online 13 April 2017


**Fig. 1.** (Blue: electrode; red: spacer; yellow: patternable fluid.) (A) no applied voltage. (B) initial instability. (C) fully-evolved structure. (For interpretation of the references to colour in this figure legend, the reader is referred to the web version of this article.)

electrostatic stress and capillary pressure means that a certain wavelength, characteristic of the fabrication parameters, grows most quickly and dominates the overall structure and centre-to-centre spacing of the final column array.

In comparison to other methods, the simplicity of this technique is a great advantage and it has the potential to produce patterns on the micro- and nanoscales without the need for expensive lithographic equipment. Functional surfaces using EHD patterning have already been produced, such as substrates for surface-enhanced Raman scattering spectroscopy (SERS), micro lens arrays and surfaces for use in vapour sensors [8–10].

In addition to its simplicity, EHD patterning technique is very versatile: any fluid can potentially be used, and although a variety of substances other than thermoplastics have been examined, there are still a great many materials that could be tested. The process itself offers a number of readily-modified parameters that may be used to provide control over the patterns produced.

Previous work in this area has both used plain, unpatterned electrodes and electrodes with a patterned surface of raised conductors. Using plain electrodes, EHD patterns in thermoplastics (PMMA and PS) with wavelengths of 2–3 μm have been produced. However, the heights of these patterns, limited by the electrode spacing, were between 200 and 500 nm, creating disks rather than pillars such as those of Schäffer et al. and Lau and Russel [4,11,12]. Other research by Dickey et al. has used plain electrodes to pattern a photocurable polymer, creating wavelengths of around 17 μm with disk heights of 2.5 μm [6].

When a patterned electrode is used, the raised patterning creates areas between the electrodes where the electric field is greater. The long-range order of the pattern can be controlled in this way, which may be advantageous for some applications, but processing the patterned electrodes can be expensive and requires specialist equipment. Patterned electrodes have been used with thermoplastics by Wu et al., who created disks with wavelengths of about 4–5 μm and heights around 200 nm in PMMA [13]. Sol-gel precursors have been used with patterned electrodes to produce inorganic oxide features with wavelengths around 2.5 μm and a height of 38 nm [5].

The objective of the present work was to use EHD instabilities to produce micro-patterned surfaces without the use of photomasks, since to some extent the benefit of the technique is vitiated by the use of electrodes that need to be patterned by photolithography. Our study has explored the scope for scale reduction of the patterns that can be obtained using simple flat plate electrodes with a room-temperature curing epoxy resin as the patternable polymer and air as the gap material.

This paper describes a method for patterning a two-part epoxy resin at the micro-scale by a simple benchtop method that could be replicated in any laboratory. A comparison of the practical results with those derived from current theory is also presented. Some effects that interfere with the production of a regular array of columns are also reported and discussed, such as the coarsening of the patterns and some possible reasons for this phenomenon.

## 2. Materials and methods

The basic experimental cell had a simple flat-plate capacitor configuration, as shown in Fig. 1. The cell was approximately 20 mm × 20 mm in basal area.

### 2.1. Patternable polymer

Many EHD patterning studies reported by other groups have used thermoplastic polymers which require a heating and cooling cycle to process the polymer. In some cases, where high molar mass polymers were used, patterning took several days to complete [4,12]. UV-curing polymers have been tested to overcome the need to heat the substrate, although they clearly need a UV source [6], and the polymers can be expensive and sensitive to ambient light. In this study, Bostik Evo-Stik Control® epoxy resin was used as the patternable fluid (Fig. 1a). It is a two-part commercial resin that does not require thermal or UV curing, with a nominal setting time of 2 h at room temperature.

The two components of the resin were very viscous, so in order to obtain a homogeneous spin-coatable liquid, they were dissolved in a solvent and then spin-coated. The hardener fully dissolved in toluene, whereas the resin would only dissolve fully in acetone. Therefore each part was dissolved in the appropriate solvent and then the two solutions were combined (to give the recommended 1:1 ratio) and freed from traces of suspended matter using a 0.22 μm filter. The mixed solution was then capable of being spin-coated and the thickness of the coating was controlled by adjusting the viscosity of the initial solutions and the spin speed (1000–4500 rpm). The viscosity was of course dependent on the concentration of the solution, which ranged from 150 to 320 g $L^{-1}$. Smooth, homogeneous layers of resin with thicknesses ranging from 0.1 to 40 μm were prepared in this way.

### 2.2. Electrode fabrication

The bottom electrodes of the EHD cell were constructed from n-type doped silicon wafers (conductivity typically 100 S $m^{-1}$), and

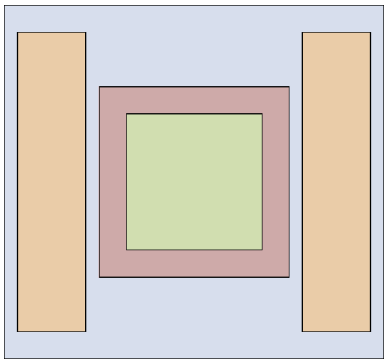

**Fig. 2.** Bottom electrode configuration. Blue: glass slide; pink: etched ITO; orange: spacer; green: epoxy layer on top of ITO. (For interpretation of the references to colour in this figure legend, the reader is referred to the web version of this article.)

were coated with an insulating material that created the space between the electrodes. Polydimethylsiloxane (PDMS) spacers between 0.5 μm and 10 μm were spin-coated onto the silicon, using a 10:1 ratio of PDMS (Dow-Corning Sylgard® 184) base to curing agent. For thinner spacers the PDMS was diluted with hexane as required. Once the PDMS coatings had been cured, the central areas of the films were removed with a razor blade to produce two bands which acted as the spacers. For the thicker spacers, up to 50 μm, epoxy resin was used in the same way and in some cases very thin layers of PS or PMMA, deposited from toluene solutions, were used.

The top electrode was a conductive (10 Ω/sq.) indium-tin oxide (ITO)-coated glass slide. An area of 10 mm × 10 mm in the centre of the thin ITO film was masked, and the outside edges were removed by etching with 1 mol $L^{-1}$ hydrochloric acid. This meant that there was no route through the spacer material for stray current to be conducted between the electrodes. The liquid epoxy resin was spun onto the ITO in the centre of the electrode, and suitable masking was used to ensure that no epoxy came into contact with the spacer material (Fig. 2).

For experiments in which the potential difference was below 60 V, a variable-voltage DC power supply was used. For higher-voltage experiments, a 400 V source was used, with a large current-limiting resistor (15 MΩ) in the circuit for safety; due to small leakage currents in the cell, this reduced the source voltage to a smaller measured value across the capacitor. Since the polymer was solidified by room-temperature curing, no heat source was required.

An Olympus LEXT 3D laser measuring microscope OLS 4100 was used to examine the dimensions and structure of the fabricated surfaces, epoxy layers and spacers.

## 3. Results and discussion

Surfaces were produced using a variety of experimental parameters, with spacer thicknesses ranging from 0.1 to 46 μm. Voltages ranging from 30 to 162 V were applied to the electrodes, and were maintained for about 4 h, to ensure that the epoxy was fully cured before removing the sample.

Fig. 3 shows an instability pattern forming. Small thermal perturbations at the fluid surface couple to the electrically-induced instability, and isolated disks develop within the gap [14]. Each one destabilises the fluid around it, and more disks then form around the initial instability, eventually covering the entire surface. The disks become elongated into pillars, which grow towards the opposite electrode.

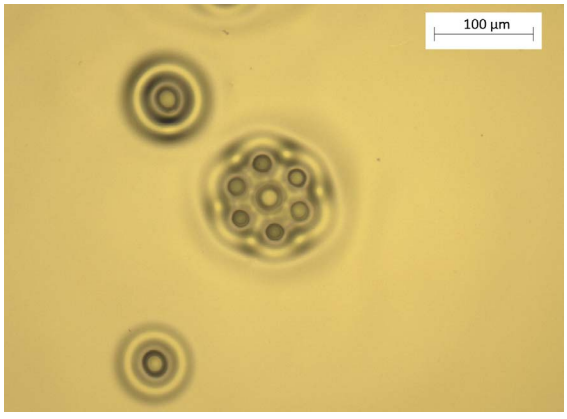


**Fig. 3.** Optical micrograph showing a quasi-hexagonal patterned array forming around a central pillar. Pattern height: 26.6 μm.

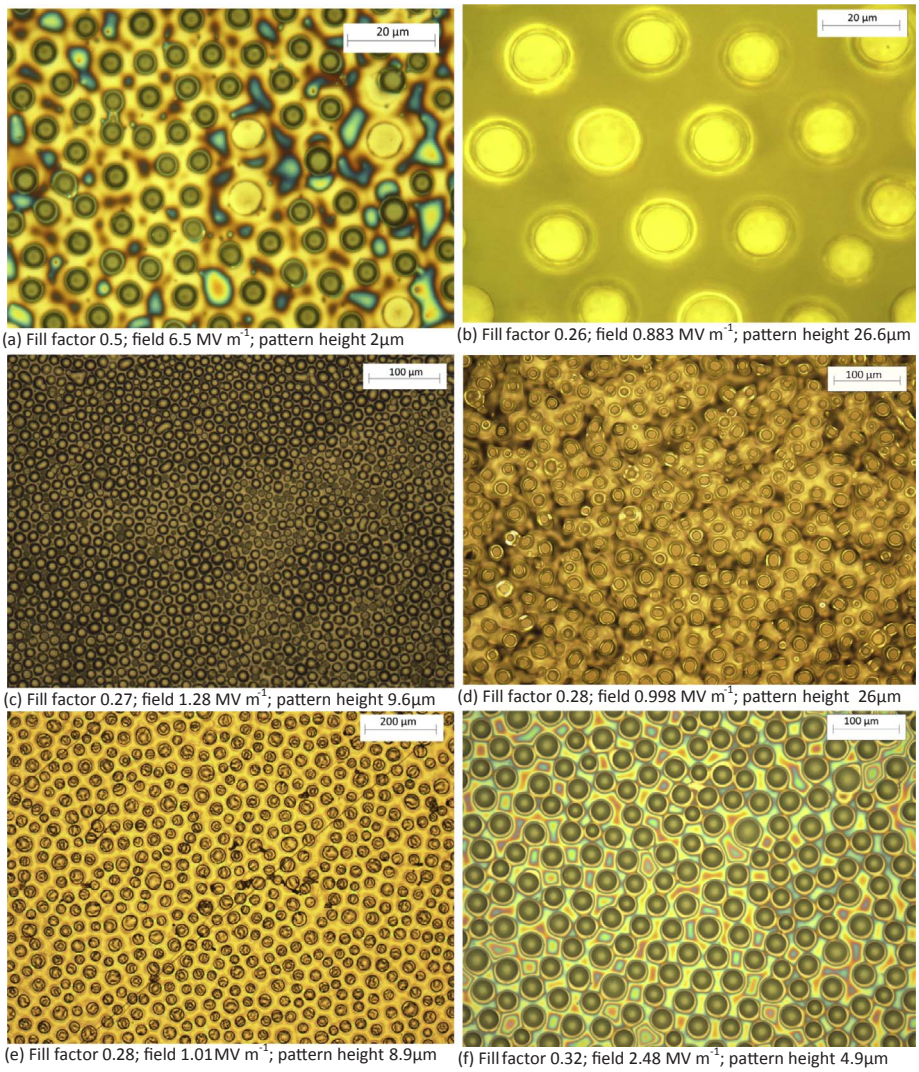


(a) Fill factor 0.5; field 6.5 MV m$^{-1}$; pattern height 2µm
(b) Fill factor 0.26; field 0.883 MV m$^{-1}$; pattern height 26.6µm
(c) Fill factor 0.27; field 1.28 MV m$^{-1}$; pattern height 9.6µm
(d) Fill factor 0.28; field 0.998 MV m$^{-1}$; pattern height 26µm
(e) Fill factor 0.28; field 1.01MV m$^{-1}$; pattern height 8.9µm
(f) Fill factor 0.32; field 2.48 MV m$^{-1}$; pattern height 4.9µm

**Fig. 4.** EHD instability patterns in epoxy resin with the stated fill factors and electric fields.

### 3.1. General results

Arrays with short-range order were produced and, as expected from the literature, each pillar normally had 6 nearest neighbours, leading to the quasi-hexagonal patterns shown in Fig. 4a, b, c and f. Some samples displayed very little apparent order, although the average packing density of the columns was quite constant (Fig. 4d & e). The scale (average spacing or wavelength) of the resulting patterns could be altered by changing the fabrication parameters, including the applied voltage, resin film thickness and electrode gap. Relevant parameters for the samples illustrated in Fig. 4 are the fill factor (the ratio of the epoxy thickness to the spacer gap, so a completely-filled gap would have a fill factor of 1) and the electric field in the epoxy (higher fields typically producing smaller-scale patterns).

Models of EHD patterning generally consider two regimes: the polymer being patterned is either regarded as a perfect dielectric, so that only polarisation of partial charges occurs, or as a leaky dielectric, in which case some mobile charges accumulate at the interface. A number of models have been produced, generally under the simplifying assumption of the lubrication approximation; those used here are the perfect dielectric model propounded by Schäffer et al. [4], and the leaky and perfect dielectric models given by Pease and Russel [15]. Their equations indicate that altering the experimental parameters offers a large degree of control over the patterns produced, and a very wide range of sizes is possible. The wavelength λ (or mean spacing of the pillars) predicted by the perfect dielectric model of Schäffer et al. is given in Equation (1):

$$\lambda = 2\pi\sqrt{\frac{\gamma U}{\varepsilon_0\varepsilon_p(\varepsilon_p-1)^2}}\left[\frac{U}{\varepsilon_p d-(\varepsilon-1)h}\right]^{\frac{-3}{2}} \tag{1}$$

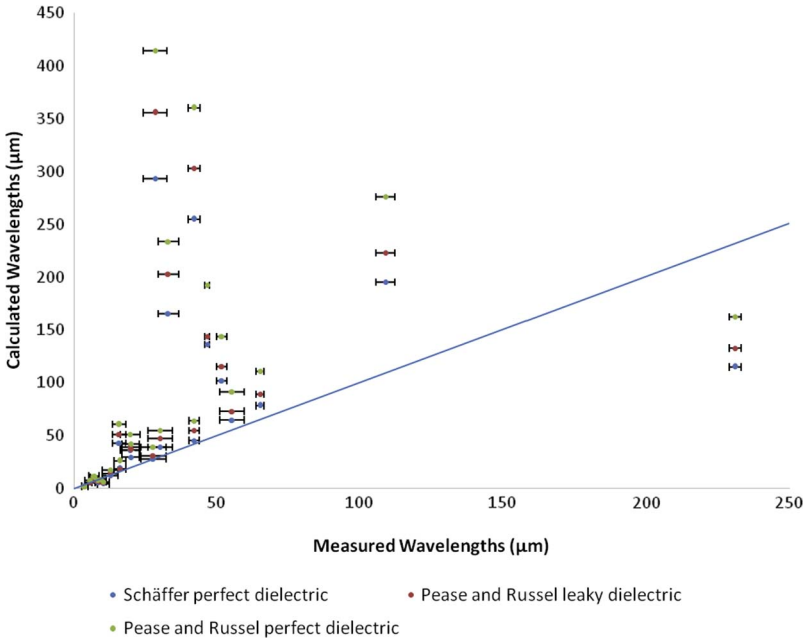


**Fig. 5.** Graph of measured experimental results vs theoretically predicted values for the corresponding experimental parameters, taking $\varepsilon_p$ to be 9.0.

where U is the voltage, surface tension is $\gamma$, the relative permittivity of a vacuum is $\varepsilon_0$, the relative permittivity of the liquid is $\varepsilon_p$, $d$ is the electrode spacing and $h$ is the liquid film thickness.

The leaky dielectric model developed by Pease and Russel [15] predicts that the wavelength of the pattern $\lambda$ is given by:

$$\lambda = \frac{2\sqrt{2}\pi\gamma^{\frac{1}{2}}(d-h)^{\frac{3}{2}}}{|U|(\varepsilon_0\varepsilon_1)^{\frac{1}{2}}} \tag{2}$$

where $\varepsilon_1$ is the relative permittivity of air.

The pillar spacing for a perfect dielectric according to Pease and Russel is given by:

$$\lambda = \frac{2\sqrt{2}\pi\gamma^{\frac{1}{2}}[\varepsilon_1 h_0 + \varepsilon_2[(d-h)]]^{\frac{3}{2}}}{|U|(\varepsilon_0\varepsilon_1\varepsilon_2)^{\frac{1}{2}}[\varepsilon_2-\varepsilon_1]} \tag{3}$$

where $\varepsilon_2$ = relative permittivity of the polymer film.

In the literature, the reported film thicknesses and electrode spacings are typically much smaller than many of those used here (up to about 2 µm) [4,5,11,16–18]. Since the models were developed to describe scenarios such as the use of a thermoplastic melt, with electrode gaps and thin films of 1 µm or less, it is reasonable to suggest that they may not apply to the present work. In our experiments, the smallest wavelengths were obtained with film thicknesses between 0.3 and 3 µm and electrode spacings between 0.9 and 3.6 µm. The larger wavelengths were produced with electrode spacings up to 50 µm and epoxy thicknesses up to 15 µm. For a wide range of fabrication parameters, a comparison between the measured wavelengths and the theoretical values for the same parameters is shown in Fig. 5. (The line $y = x$ is also given for comparison).

For wavelengths below approximately 15 µm, the theoretical and measured values are in good agreement (within experimental error). Above 15 µm, the values diverge, and the difference between them is quite large. For the shorter wavelengths, the predicted values are often less than the measured ones, as shown in Fig. 6. As was pointed out by Russel et al. [15], Schäffer's model [4] predicts the smallest values.

In Fig. 7, the ratios of the predicted wavelengths to the measured ones are plotted against the electric field intensities in the polymer. Most of the theoretical predictions are within a factor of 2 of the measured values, but the divergence is large at the lowest electric fields. It seems that there may be a built-in electric field of about 1 MV $m^{-1}$ (or 1 V $\mu m^{-1}$), even in the absence of an applied voltage; such a field could plausibly be due to contact potentials at the polymer film surface.

The calculated wavelength values were based on theories which assume that the lubrication (or thin film) approximation is applicable. This approximation assumes that the characteristic length scale of the electrohydrodynamic instability is much greater than the polymer film thickness. A number of studies have indicated that the use of high fields invalidates this approximation [14,15]. Some of the fields used in the experiments presented here were quite high in comparison to other studies, and so in a number of cases the scale of the instability was comparable to the polymer thickness and the electrode spacings. This may have contributed to the disagreement with the calculated values, since the theory presented by Pease and Russel implies that deviation from the lubrication approximation results in smaller pillar spacings [15].

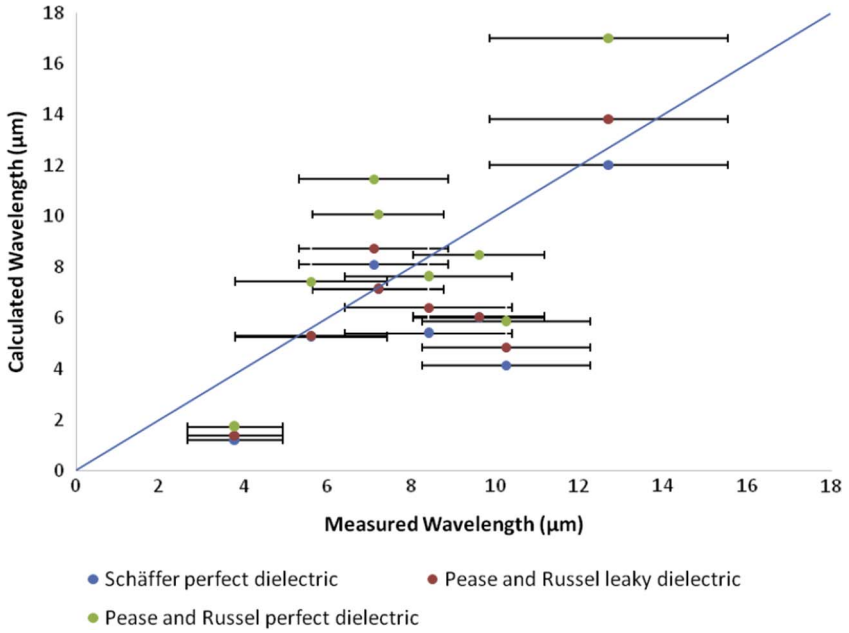


**Fig. 6.** Graph of experimental results vs. theoretical values for wavelengths below 15 µm.

### 3.2. Changing the scale of the instability

#### 3.2.1. Impact of the relative permittivity

The difference between the electric field in the liquid resin and that in the air causes an electrostatic pressure at the interface, and consequent surface deformation. In order to achieve finer patterning (i.e. to reduce the wavelength of the instability), the electric field difference can be increased by manipulating the relative permittivity of the fluid. Other workers have done this by the inclusion of a filler material such as gold nanoparticles, which reduced the wavelength by around 16% [16]. According to the perfect dielectric model, the initial benefit of this approach rapidly decreases as the relative permittivity becomes greater; this is consistent with results of Bae et al. [16], who found that increasing the volume fraction of nanoparticles in the polymer above 0.5% had a diminishing effect on the reduction of the wavelength.

For a fixed electrode gap, polymer thickness and applied voltage, both Schäffer's and Pease and Russel's perfect dielectric equations predict that increasing the relative permittivity above 4 has a rapidly-diminishing influence on the wavelength reduction. (Pease and Russel's equation for a leaky dielectric does not contain the relative permittivity of the polymer).

The relative permittivity of the epoxy resin used in this study changed throughout the duration of its curing time. This change was measured, as it could potentially affect the wavelength of the instability. The relative permittivity of a material can be derived indirectly from the capacitance (C) value using:

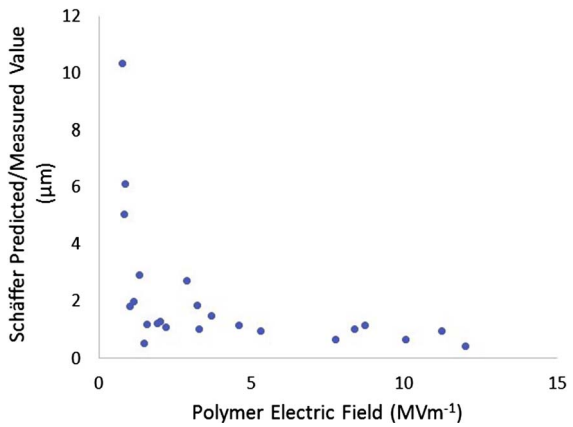


**Fig. 7.** Plot of the ratio of predicted to measured wavelengths *vs.* the polymer electric field. (A perfect dielectric sample with a relative permittivity of 9.0 was assumed.)

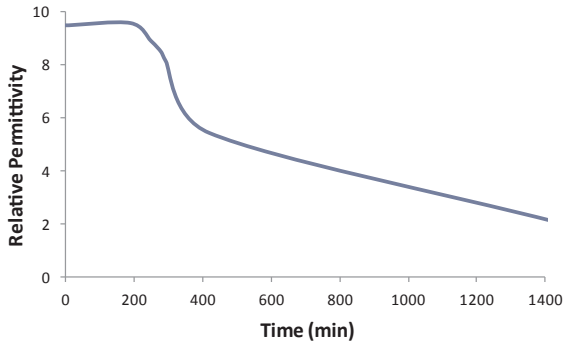


**Fig. 8.** Graph showing the change in the relative permittivity of the epoxy resin as a function of curing time.

$$Capacitance\ C = \frac{\varepsilon_p \varepsilon_0 A}{d} \tag{4}$$

where A is the area of the capacitor and d the gap between the plates.

The capacitance of a 20 mm × 20 mm square, 3 mm thick block of epoxy resin constrained within rubber washers was measured over a period of several hours at a frequency of 1 kHz. The relative permittivity was found to be about 9 for the uncured liquid (i.e. during the pattern formation stage), falling to an average of 2.5 when cured (Fig. 8). The initial value is greater than those of many polymers hitherto used in EHD patterning, such as polystyrene ($\varepsilon_2 = 2.6$), so the effect of the relative permittivity in reducing the pillar size was essentially optimised for epoxy resin without the need for filler materials (if it was behaving as a perfect dielectric).

### 3.2.2. Electrode spacing and epoxy thickness

In this study the voltage, electrode spacing and epoxy thickness were varied to produce a range of pattern scales. Since the initial relative permittivity of the epoxy was found to be high, altering the geometry of the experiment was the most effective way of reducing the wavelength of the instability. A number of previous studies have used patterned or masked electrodes to produce small

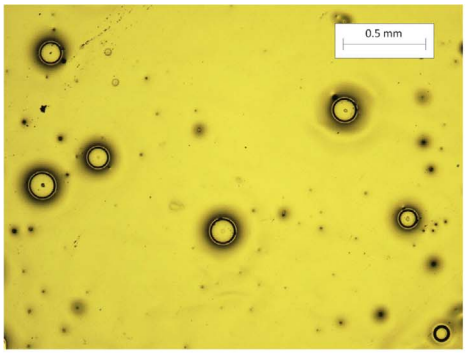


(a) Epoxy fill factor 0.53; field 2.35 MV $m^{-1}$ ; pattern height 17µm

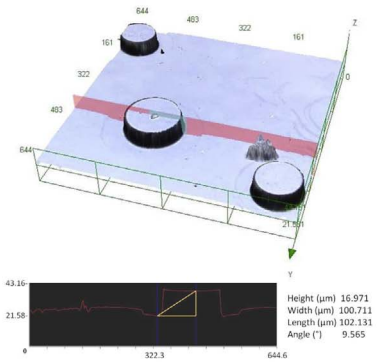


(b) Lext 3D view; scale is in µm

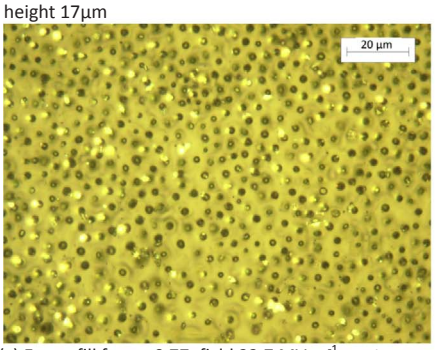


(c) Epoxy fill factor 0.77; field 22.7 MV $m^{-1}$; pattern height 3 µm. Lighter areas are where the epoxy disks have adhered to the top electrode and detached from the surface.

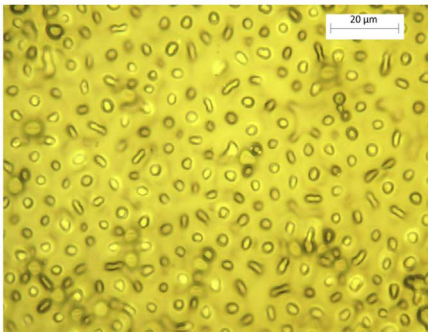


(d) Epoxy fill factor 0.6; field 8.39 MV $m^{-1}$; pattern height 3.1µm.

**Fig. 9.** Variation of wavelength values produced by the EHD patterning process.

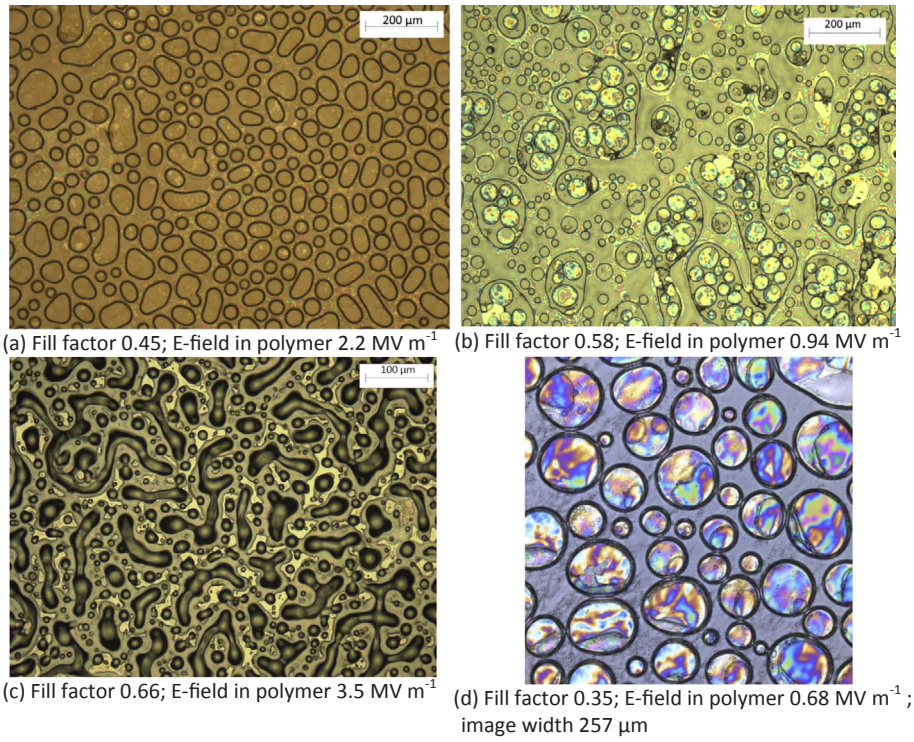


(a) Fill factor 0.45; E-field in polymer 2.2 MV $m^{-1}$

(b) Fill factor 0.58; E-field in polymer 0.94 MV $m^{-1}$

(c) Fill factor 0.66; E-field in polymer 3.5 MV $m^{-1}$

(d) Fill factor 0.35; E-field in polymer 0.68 MV $m^{-1}$ ; image width 257 µm

e. 3D view (scale in µm).

**Fig. 10.** (a) to (d) Coalesced surfaces, showing values of fill factor and polymer electric field. e: 3D view of the sample in (d).

structures and patterns [5,12,19]. The objective of this study was to produce structures via the simplest EHD patterning method without the use of more complex electrodes, and to investigate the potential of using a simple flat electrode. The range of wavelengths that was achieved is shown in Fig. 6. The wavelength of the instability in Fig. 9 a and b was in the order of several hundred µm, and the disks themselves were around 200 µm in diameter. In contrast, the wavelengths of the instabilities shown in Fig. 9 c and d were between 5 and 7 µm, each disk being 1–2 µm in diameter. As the spacer and epoxy film thicknesses became smaller, there were larger areas of disarray in the patterned surfaces. For the highest fields used in this study, a larger range of wavelengths were competing for dominance on the polymer surface, which meant that the ordering was more chaotic [15]. It also seems likely that dielectric breakdown in the polymer and air layers could become a limiting factor under very high-field conditions.

Theory predicts that the use of a leaky dielectric and the subsequent accumulation of charges at the interface will reduce the wavelength of the instability [20,21]. The current flow during our experiments was measured using a microammeter in the circuit. The measured current appeared to follow two regimes. For the experiments where the electrode gap was comparatively large (above ~7 µm), a very small leakage current (15 µA or less) was observed when the disks had contacted the top electrode. This was probably due to the mobility of trace ionic impurities in the uncured epoxy resin, and this supposition is supported by the fact that the current fell to only 0.1 or 0.2 µA once the resin had been fully cured.

The current flow in the experiments using larger spacers did not significantly affect the overall voltage drop across the capacitor, as in most cases it was very small. Given the observed current flow and also the nature of the material, i.e. an epoxy in which there could be mobile ionic residues, it seems likely that the material was not behaving as a perfect dielectric.

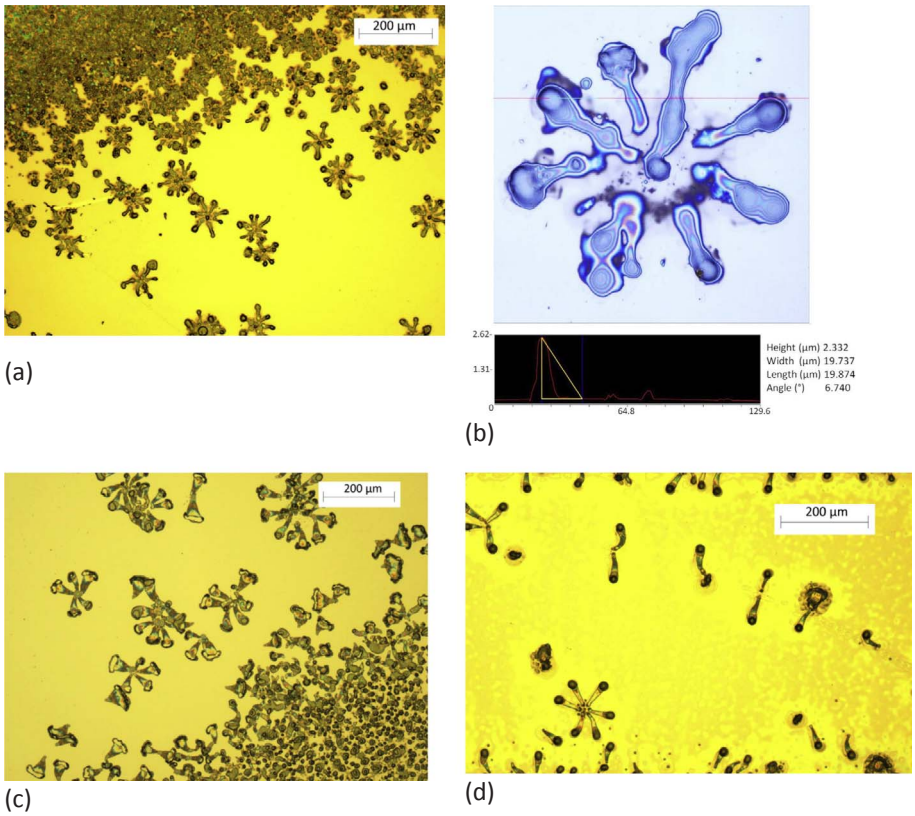


**Fig. 11.** (a) Starburst effect. Epoxy thickness 0.5 µm; spacer 2.3 µm. (b) 3D LEXT examination of the epoxy patterns left on the two electrodes, showing that the material had fanned out whilst being in contact with both electrodes. (c) Starburst effect. (d) Starburst and traversing pillars.

A greater leakage current flow of 15 µA or more was observed when the spacer gap was below 7 µm. Stray currents were often observed before the patterning actually took place, and these currents appeared routinely when the spacer gap was below 2 µm. This was likely to be due to conduction through the air and/or epoxy layers (dielectric breakdown), or to impurities in the device, and it often reached the full current compliance of the circuit. The electrical breakdown of air occurs at field intensities of ~3 MV $m^{-1}$, and it could limit the attainable resolution scale of the patterns.

Lau and Russel proposed that the breakdown of both the polymer and the air occurred during their EHD patterning experiments with thin films of PMMA, causing both disorder in the patterns and experimental wavelengths that were larger than the theoretical values [11]. Whilst the thicknesses of the spacers and films that those authors used were less than 200 nm, it could also be that breakdown of the layers was occurring in our own experiments with the smallest spacings (producing fields in excess of $10^7$ $Vm^{-1}$). Lau and Russel found that the smallest wavelengths obtainable rarely fell below 1 µm, even when such values were predicted by theory; certainly when the aim of these experiments was to produce smaller wavelengths, this was found to be difficult to achieve, due to the flow of significant electrical currents [11].

The observation of current flow when the pillars had grown across the electrode gap tends to support the proposition that the epoxy was behaving as a leaky dielectric before it had cured [15]. The breakdown of the two layers that seems to have occurred might at least partly explain the discrepancy between the measured results and theoretical ones.

### 3.3. Other effects

#### 3.3.1. Coalescence

The EHD patterning process itself is dynamic and continues until the fluid is solidified, even when the voltage is removed. The formation of pillars reduces electrostatic stress at the interface but increases the overall surface energy which tends to become minimised due to thermodynamic factors. As a result, if certain geometric requirements are fulfilled, the disks coalesce over time and lose a semi-ordered pattern. A fill factor of 0.75 leads to coalescence very quickly, whereas for a fill factor $< 0.25$, hexagonal arrays form and remain more stable [22]. Modelling has indicated that increasing the fill factor also increases the disorder until, at $> 0.75$, coalescence occurs very rapidly [22]. This can be seen in Fig. 10a, where the smaller, more evenly-sized disks have combined to form shapes that are larger and more elliptical. As the pattern continues to evolve, phase inversion can occur, as shown in Fig. 10b and c, where lines and circular columns of air surrounded by liquid are visible, along with the smaller epoxy disks. Complete phase inversion has occurred in Fig. 10c and d. Kim and Lu demonstrated numerically that keeping all other parameters constant, a thicker

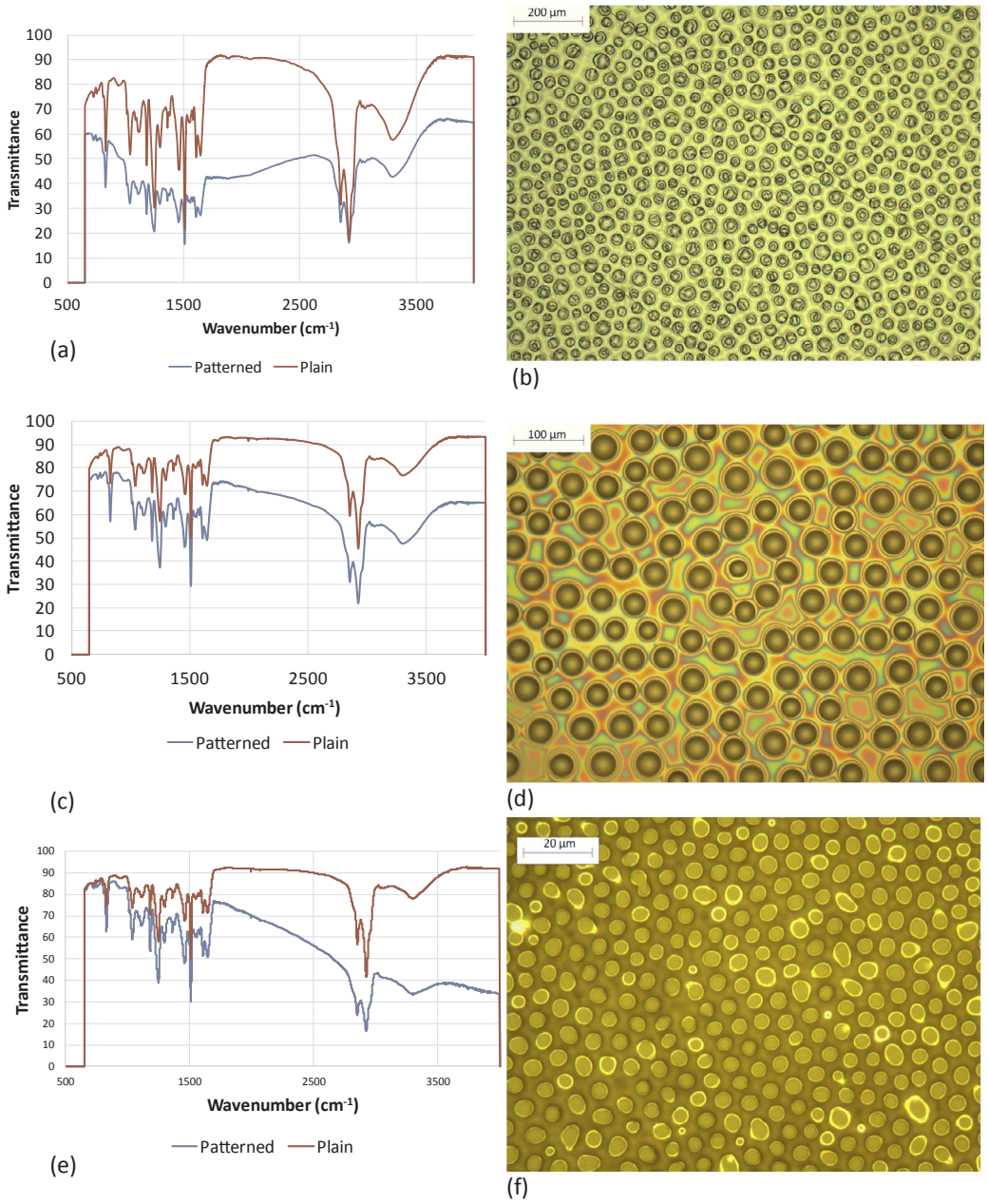


**Fig. 12.** IR transmission spectra ((a), (c) and (e)) of the patterned surfaces and plain epoxy surface and their corresponding surfaces shown on the right ((b), (d) and (f)).

film produced more densely packed pillars and increased the growth rate; they also found that (due to the excess material) coarsening was more likely to occur [23]. All the fill factors in the surfaces shown in Fig. 10 are over 0.25, with the highest being 0.66, and it is clear that they were all liable to produce coalescence and coarsened patterns given enough time.

### *3.3.2. Starburst patterns*

Fig. 11 shows disks that have spread laterally across the electrode surface, which to the best of our knowledge has not been reported previously. From the starburst patterns that were formed, it appears that the pillars repelled one another. An examination of the two electrodes showed that the pillars moved away from one another once they had grown across the gap and were in contact with both electrodes. This was possibly due to a build-up of charge on the surface of the liquid epoxy pillars, as would occur with a leaky dielectric material. These patterns tended to form when the spacer gap and epoxy thickness were below approximately 3.5 µm. Since this effect occurred when the geometry of the experiment was small, it could tend to limit the ability to produce nanoscale patterns in this kind of material, so a fuller understanding of the process would be useful.

### 3.4. Infrared transmission spectra

The interaction between the surfaces and IR radiation was investigated. Moulds of the EHD patterns were fabricated in PDMS. These were then used to replicate the surfaces, in epoxy, over larger areas on NaCl disks which were transparent to the infrared wavelengths used (20–2.5 μm).

The IR transmission spectra for three surfaces are shown in Fig. 12, and compared with that of plain, unpatterned epoxy. There is no obvious change in the vibrational bands. However, patterned and regularly-textured surfaces can interact with wavelengths of light that are comparable to the size of the surface patterns, via multiple reflections between the features. A drop in transmission through the patterned surfaces in comparison to the unpatterned epoxy can be seen, peaking at higher wavenumbers as the scale of the pillar features becomes smaller, as would be expected. However, for the sample shown in Fig. 12a, the wavelength of maximum interaction (around 5 μm, or 2000 $cm^{-1}$) is smaller than expected, given the wavelength of the pillars themselves. Nevertheless, there are other features on the surface which are roughly comparable in size to the IR wavelengths, such as the gaps between the pillars and texturing on top of the pillar: this is true of the sample in Fig. 12c also. The surface shown in Fig. 12f contains features (the gaps between the structures) which are also comparable in scale to the peak wavelength ($< 2.5$ μm, or $> 4000$ $cm^{-1}$).

## 4. Conclusion

This study has shown that room-temperature curable epoxy resin can be successfully utilised to produce arrays of ordered and disordered structures (especially disks and pillars) via electrohydrodynamic instability patterning. Anomalies such as the disagreement between the measured and calculated wavelengths, and the star shapes that were produced with small electrode gaps, indicate that the epoxy should not be modelled as a perfect dielectric; they may imply that mobile ionic charges in the uncured resin should be taken into account in the modelling, especially when attempting to optimise the EHD patterning of epoxy with a flat electrode. Finally, the IR spectroscopic data indicate that the patterned surfaces interact strongly with the incident IR beam. The mechanism of this interaction and the possible utility of simple EHD pillaring of curable resins for optical applications such as broad-band antireflection layers are under investigation. The patterned, fully-cured epoxy surfaces also appear to have desirable properties for use as cell-culture surfaces with controlled cell-cell interactions [24].

Future work to increase the resolution of the EHD-patterned epoxy layers will also need to consider the use of patterned electrodes and possibly ac electric fields.

## Acknowledgements

We are grateful to Kingston University London for the provision of a Bursary for C.H.T. We also thank Prof. P. Spearman for a helpful discussion.

## References

[1] Y. Li, G. Huang, X. Zhang, L. Wang, Y. Du, T. Lu, et al., Engineering cell alignment in vitro, Biotech. Adv. 32 (2014) 347–365.
[2] I. Khodasevych, L. Wang, A. Mitchell, G. Rosengarten, Micro- and nanostructured surfaces for selective solar absorption, Adv. Opt. Mater. 3 (2015) 852–881.
[3] L. Mishchenko, B. Hatton, V. Bahadur, A. Taylor, T. Krupenkin, J. Aizenberg, Design of ice-free nanostructured surfaces based on repulsion of impacting droplets, ACS Nano 4 (2010) 7699–7707.
[4] E. Schäffer, T. Thurn-Albrecht, T. Russell, U. Steiner, Electrohydrodynamic instabilities in polymer films, Europhys. Lett. 53 (2001) 518–524.
[5] N. Voicu, M. Saifullah, K. Subramanian, M. Welland, U. Steiner, $TiO_2$ patterning using electro-hydrodynamic lithography, Soft Matter 5 (2007) 554–557.
[6] M. Dickey, E. Collister, A. Raines, P. Tsiartas, T. Holcombe, S. Sreenivasan, et al., Photocurable pillar arrays formed via electrohydrodynamic instabilities, Chem. Mater. 18 (2006) 2043–2049.
[7] N. Wu, W. Russel, Micro- and nano-patterns created via electrohydrodynamic instabilities, Nano Today 4 (2009) 180–192.
[8] S. Mahajan, U. Steiner, P. Goldberg-Oppenheimer, Hierarchical electrohydrodynamic structures for surface-enhanced Raman scattering, Adv. Mater. 24 (2012) OP175–OP180.
[9] Y.-J. Lee, Y. Kim, Y.-K. Kim, C.-Y. Yu, J.S. Gwag, J.-H. Kim, Microlens array fabricated using electrohydrodynamic instability and surface properties, Opt. Express 19 (2011) 10673.
[10] X. Yan, G. Liu, M. Dickey, G. Willson, Preparation of porous polymer membranes using nano- or micro-pillar arrays as templates, Polymer 45 (2004) 8469–8474.
[11] C. Lau, W. Russel, Fundamental limitations on ordered electrohydrodynamic patterning, Macromolecules 44 (2011) 7746–7751.
[12] M. Morariu, N. Voicu, E. Schäffer, Z. Lin, T. Russel, U. Steiner, Hierarchical structure formation and pattern replication induced by an electric field, Nat. Mater. 2 (2003) 48–52.
[13] N. Wu, L. Pease, W. Russel, Toward large-scale alignment of electrohydrodynamic patterning of thin polymer films, Adv. Func. Mater. 16 (2006) 1992–1999.
[14] P. Gambhire, R. Thaokar, Role of conductivity in the electrohydrodynamic patterning of air-liquid interfaces, Phys. Rev. E 86 (2012) 036301.
[15] L. Pease, W. Russel, Limitations on length scales for electrostatically induced submicrometer pillars and holes, Langmuir 20 (2004) 795–804.
[16] J. Bae, E. Glogowski, S. Gupta, W. Chen, T. Emrick, T. Russell, Effect of nanoparticles on the electrohydrodynamic instabilities of polymer/nanoparticle thin films, Macromolecules 41 (2008) 2722–2726.
[17] S. Manigandana, S. Majumder, A. Suresh, S. Ganguly, K. Kargupta, D. Banerjee, Electric field induced dewetting and pattern formation in thin conducting polymer film, Sens. Actuat. B: Chem. 144 (2010) 170–175.
[18] Z. Lin, T. Kerle, T. Russell, E. Schäffer, U. Steiner, Structure formation at the interface of liquid/liquid bilayer in electric field, Macromolecules 35 (2002) 3971–3976.
[19] X. Li, Y. Ding, J. Shao, H. Tian, H. Liu, Formation of arbitrary patterns in ultraviolet cured polymer film via electrohydrodynamic patterning, Sci. World J. (2014) 9840497, , , http://dx.doi.org/10.1155/2014/840497.
[20] V. Shankar, A. Sharma, Instability of the interface between thin films subjected to electric fields, J. Colloid Interface Sci. 274 (2004) 294–308.
[21] S. Roberts, S. Kumar, AC electrohydrodynamic instabilities in thin liquid films, J. Fluid Mech. 631 (2009) 255–279.
[22] R. Verma, A. Sharma, K. Kargupta, J. Bhaumik, Electric field induced instability and pattern formation in thin liquid films, Langmuir (2005) 3710–3721.
[23] D. Kim, W. Lu, Interface instability and nanostructure patterning, Comput. Mater. Sci. (2006) 418–425.
[24] C.H. Trease, M.R. Longman, A.T. Augousti, P.J.S. Foot, B. Pierscionek, Cell morphology and growth observation studies on novel, chemically unmodified and patterned polymer surfaces for advanced tissue culture applications, Polymer 109 (2017) 13–24.